UHASSELT
KNOWLEDGE IN ACTION

Maastricht University

Faculty of Medicine and Life Sciences
School for Life Sciences
Master of Biomedical Sciences

Master's thesis

Forever Young - The Epigenetic Clock of OPCs in Multiple Sclerosis

Freddy Leenders

Thesis presented in fulfillment of the requirements for the degree of Master of Biomedical Sciences, specialization Molecular Mechanisms in Health and Disease

SUPERVISOR :

Prof. Daniel VAN DEN HOVE

2023
2024

Transnational University Limburg is a unique collaboration of two universities in two countries: the University of Hasselt and Maastricht University.

UHASSELT
KNOWLEDGE IN ACTION

www.uhasselt.be
Universiteit Hasselt
Campus Hasselt:
Martelarenlaan 42 | 3500 Hasselt
Campus Diepenbeek:
Agoralaan Gebouw D | 3590 Diepenbeek

Maastricht University

Faculty of Medicine and Life Sciences
School for Life Sciences
Master of Biomedical Sciences

Master's thesis

Forever Young - The Epigenetic Clock of OPCs in Multiple Sclerosis

Freddy Leenders

Thesis presented in fulfillment of the requirements for the degree of Master of Biomedical Sciences, specialization Molecular Mechanisms in Health and Disease

SUPERVISOR :

Prof. Daniel VAN DEN HOVE

Forever Young – The Epigenetic Clock of OPCs in Multiple Sclerosis

Freddy Leenders[1,2], Assia Tiane[1,2,3], Lisa Koole[1,2,3], Inez Wens[1,2,3], Daniel van den Hove[2], Tim Vanmierlo[1,2,3]

[1]Department of Neuroscience, Biomedical Research Institute, Faculty of Medicine and Life Sciences, Hasselt University, Diepenbeek, Belgium.
[2]Department Psychiatry and Neuropsychology, Division Translational Neuroscience, Mental Health and Neuroscience Research Institute, Maastricht University, Maastricht, the Netherlands.
[3]University MS Centre (UMSC) Hasselt, Pelt, Belgium.

*Running title: *The role of OPC aging in multiple sclerosis*

To whom correspondence should be addressed: Tim Vanmierlo, Tel: +32 11 26 92 28; Email:tim.vanmierlo@uhasselt.be

Keywords: DNA methylation, Aging, senescence, myelination, multiple sclerosis

ABSTRACT

Although multiple sclerosis (MS) typically manifests between the ages of 20 and 40, premature aging has emerged as a significant contributor to disease progression. Despite previous research indicating the significant impact of aging on oligodendrocyte precursor cell (OPC) differentiation, underlying mechanisms remain poorly understood. In this study, we examined differences in DNA methylation patterns between neonatal and aged mouse OPCs, juxtaposing our findings with differentially methylated genes between chronic inactive lesions and normal-appearing white matter (NAWM). Our analysis revealed 12,353 differentially methylated genes between neonatal and aged mouse OPCs. Upon comparison with MS brain samples, we identified 469 overlapping genes, including 18 genes known to be associated with aging. Notably, SIRT2, a deacetylase, exhibited a strong correlation between methylation and gene expression levels, being downregulated in MS lesions relative to NAWM. Additionally, global methylation analysis of control versus MS brain samples showed a trend towards accelerated epigenetic aging in lesions. While markers of cellular senescence, P16 and P21 were differentially methylated in aged mice but not in MS brain samples, our investigation revealed increased P16 levels in OPCs within remyelinated lesions, and an increasing trend in chronic lesions. Lastly, we established an in vitro model to induce cellular aging in OPCs. Collectively, our findings demonstrate that aged OPCs and MS lesions exhibit hallmarks of aging at both epigenetic and gene expression levels. Furthermore, OPCs derived from MS lesions display elevated P16 levels compared to NAWM.

INTRODUCTION

With 2.9 million cases reported globally in 2023, multiple sclerosis (MS) stands out as the most prevalent demyelinating neurodegenerative disorder impacting the central nervous system (CNS) (1, 2). The myelin sheath is a protective layer surrounding our nerve fibers that ensures rapid transmission of nerve signals and provides metabolic support to the neurons (1, 3). In MS the myelin sheath is compromised by an autoimmune reaction against myelin proteins, rendering nerves vulnerable to damage and impairing nerve conduction. Relapsing-remitting MS, constitutes 87% of MS diagnoses. Relapses involving the breakdown of myelin, a process termed demyelination, alternate with periods of remission. During remission neural repair occurs and new myelin is produced to replace the damaged myelin sheath, a process called remyelination. Symptoms vary widely and may include blurred vision, muscle weakness, lack of coordination, sensory issues, fatigue, and numbness (4). As the disease progresses into secondary progressive MS (SPMS), demyelination and nerve damage persist without periods of repair, leading to a gradual worsening of neurological symptoms and disability accumulation (5, 6). A minority of patients experience a progressive disease course

immediately from its onset, termed primary progressive MS (PPMS) (6).

The process of remyelination is initiated by the recruitment of oligodendrocyte precursor cells (OPCs) to the lesion area. Within lesions, OPCs differentiate into a new pool of mature oligodendrocytes (OLs), the myelinating cells of the CNS. Newly formed OLs, along with pre-existing OLs generate new myelin to replace damaged myelin sheaths. The contribution of pre-existing OLs to remyelination is somewhat controversial and may vary depending on species (7, 8). As the disease progresses towards PMS, remyelination fails due to impaired OPC differentiation, leaving demyelinated lesions unrepaired and susceptible to further degeneration (5, 9). Existing MS treatments, known as disease-modifying therapies (DMTs), mainly focus on suppressing the abnormal immune response in order to prevent further damage to the myelin sheath and nerves, yet are unable to halt disease progression. Driving remyelination is therefore considered as the anchor point for new therapeutic strategies in MS (10). Despite great efforts and promising preclinical studies, so far, drugs targeting remyelination prove ineffective in clinical settings, often due to translational challenges and disease heterogeneity. While it is recognized that impaired OPC differentiation is the primary cause for remyelination failure, the exact underlying mechanisms remain poorly understood. Consequently, effectively targeting OPC differentiation to promote remyelination induces challenges (11, 12).

Recently, Both cell-intrinsic and environment-driven age-related changes have been pointed out as major contributors to reduced OPC differentiation capacity and remyelination failure in PMS (13, 14). Compromised remyelination is evident in aged rodents and zebrafish, and can be attributed to diminished and delayed repopulation of lesions with mature OLs, resulting in the formation of thinner and less myelin sheaths (15-17). Interestingly, senescence, induced by P16 and P21 has been recognized as an underlying cause for OPC differentiation failure in both mice and humans (14, 18). Changes in the aged cellular microenvironment were previously linked to the development of a senescent phenotype. Rejuvenating the micro-environment of aged OPCs with fasting mimetic metformin has been shown to enhance OPC differentiation by reducing age-related markers in aged rodent models (14). Changes in the micro-environment include stiffening of the extracellular matrix (ECM), accumulation of myelin debris, heightened oxidative stress, and elevated levels of pro-inflammatory cytokines, which collectively contribute to the failure of OPC differentiation (19-21). Environmental changes impact gene expression regulation on the epigenetic level (14, 22-24). Given the crucial role of DNA methylation in OPC differentiation and remyelination, age-related alterations in methylation patterns are likely to contribute to OPC differentiation failure (25, 26). While demyelination normally triggers increased activity of DNA-methylating enzymes DNA methyltransferase 1 (DNMT1) and DNMT3a, aged rodent-derived OPCs exhibit a global hypomethylation phenotype characterized by the downregulation of *Dnmt1* (27, 28). The depletion of *Dnmt1*/*3a* has been demonstrated to hinder OPC differentiation in adult mice, underscoring the role of DNA methylation in this process (29). Dysregulated *Dnmt* expression impacts glial cells residing in MS lesions, which display differential methylation at over 1200 CpG positions compared to the surrounding normal-appearing white matter (NAWM) (30). Additionally, recent evidence suggests that stem cells in PPMS lesions do also show signs of senescence, thereby influencing the epigenetic signature of OPCs. High mobility group box 1 (HMGB1), a highly conserved and ubiquitous protein, is released by neural precursor cells (NPCs) in human PPMS lesions. Upon uptake by OPCs, HMGB1 induces several epigenetic regulators (4). Rouillard et al. demonstrated in rats that HMGB1 directly inhibits OPC differentiation, thereby impairing remyelination (31).

Even though the transcriptome and proteome of aged OPCs have already been largely unraveled, and global methylation changes have been indicated, the aged OPC methylome remains undisclosed, hiding the underlying mechanism responsible for downstream transcriptional, translational and cellular changes in PMS OPCs and their inability to differentiate towards mature and functional OLs (13, 27). This study aims to unravel changes in the DNA methylation signature of aged OPCs and compare these with DNA methylation patterns of MS brain samples. Understanding the role of epigenetic aging in MS may reveal new epigenetic targets for rejuvenating aged OPCs and promoting OPC differentiation in MS. Our hypothesis suggests that both aged OPCs and OPCs in PMS are

subject to accelerated epigenetic ageing and that their specific age-related DNA methylation signature prevents their differentiation and remyelination capacity. Hence, identifying new targets to rejuvenate the epigenetic signature of aged OPCs could be a crucial first step in restoring the normal functionality of aged OPCs. A deeper understanding of the epigenetic aging process will present new opportunities for targeting and enhancing remyelination strategies for MS.

EXPERIMENTAL PROCEDURES

OPC isolation - Ethical approval for all *in vitro* mouse experiments was obtained from the Hasselt University Ethics Committee for Animal Experiments (matrix number: 202301K). All experiments used male C57BL/6 mice. Primary mouse OPCs were isolated from mixed glial cultures, obtained from cerebral cortices (one brain per sample) using the standard shake-off method. For details refer to the supplementary information.

Immunocytochemistry – Primary OPCs were seeded onto poly-D-lysine coverslips and fixed in homemade 4% paraformaldehyde (PFA) for 30 minutes. Non-specific antigens were blocked with 1% Bovine Serum Albumin (BSA) in 0.1% PBS for 30 minutes at room temperature (RT). Next, cells were incubated with primary PDGFRα and KI67/ 5mC antibodies (Table S1) diluted in blocking buffer at RT. After a four-hour incubation period, the primary antibodies were detected using Alexa 488 and 555-conjugated secondary antibodies (Table S1) for one hour at RT. Nuclei were counterstained with 4,6′ -diamidino-2-phenylindole (DAPI) (Table S1) for 10 minutes at RT. Cells were mounted using Fluoromount-G (Thermo Fisher Scientific, MA, USA) and imaged utilizing a DM2000 LED microscope equipped with a Leica MC170 HD Camera (Leica Microsystems, Diegem, Belgium). Three random images per coverslip were captured and averaged. Image analysis was performed using ImageJ-win64 software.

DNA methylation profiling (mice) – Primary OPCs were isolated from whole brains of newborn (postnatal day 0 (P0)) (nOPCs) and aged (22 months) (aOPCs) mice (1 brain per sample) using magnetic-activated cell sorting (MACS). Briefly mouse brains were mechanical and enzymatic digested using surgical equipment and papain solution (30 minutes, 37°C) (3U/ml, diluted in Dulbecco's Modified Eagle Medium (DMEM) supplemented with 1 mM L-cysteine; Sigma-Aldrich, Bornem, Belgium). Subsequently, the cell suspension was filtered through a 75 µm strainer, followed by resuspension of the resulting pellet in a solution comprising 30% SIP (9:1 ratio of percoll (Sigma-Aldrich, Belgium) and 10x phosphate-buffered saline (PBS) (Thermo Fisher Scientific, MA, USA) in DMEM. Following underlaying with 70% SIP in 1x Hanks' Balanced Salt Solution (HBSS) (With Mg2+ and Ca2+, Gibco, NY, USA) and subsequent centrifugation, the interface enriched with mononuclear cells was collected. Isolation of OPCs from the mixed mononuclear cell population was performed using MACS with anti-A2B5+ microbeads (Miltenyi Biotec, Leiden, The Netherlands), following the manufacturer's instructions. Briefly, cells were incubated with an Fc receptor (FcR) blocking agent (Purified anti-mouse CD16/32, Biolegend, CA, USA) and anti-A2B5+ microbeads (15 minutes, 4°C). After incubation, cells were washed 3 times with homemade MACS buffer prior to elution of A2B5+ cells in DMEM. Finally, cells were centrifuged at 300 g for 5 minutes, resuspended in 0.1% PBS, and stored at -20°C until further use for DNA isolation and EWAS, as described in the relevant sections. Genomic DNA (gDNA) was extracted using the DNeasy Blood & Tissue Kit (Qiagen, The Netherlands). Bisulfite conversion of gDNA was performed using the Zymo Research EZ DNA Methylation-Direct Kit (BaseClear Lab Products, Leiden, The Netherlands). Concentration and purity of the DNA samples were determined using the Qubit dsDNA HS Assay kit (Invitrogen) on the Qubit Flex Fluorometer (Thermo Fisher Scientific, USA). The Epigenomic Services from Diagenode (Liège, Belgium) performed epigenetic analysis on the bisulfite converted DNA using the Infinium™ Mouse Methylation BeadChip (285K). Differential methylation analysis was performed using RStudio (version 2023.12.0). Quality control procedures were implemented using the Sensible Step-wise Analysis of DNA Methylation (SeSAMe) Beadchips package (32) along with a customized R workflow developed by Dr. Joe Burrage at the University of Exeter, UK. All 16 samples met the following criteria: median signal intensity >2000, bisulfite conversion percentage >80%, correct prediction of sex and mouse strain, Single nucleotide polymorphism (SNP) allele frequencies <0.9,

probe detection p-values >0.05 and were retained for further analysis. Methylation values were computed as beta values ([methylation intensity / (methylated intensity + unmethylated intensity + 100)]) and normalized using the Beta MIxture Quantile dilation (BMIQ) strategy. Beta values were converted to M values for differential methylation analysis. Principal component analysis (PCA) was utilized to assess the total variation in M-values attributed to age, chip number, and chip position. Differential methylation analysis was conducted on the M-values using the Limma package in R (33). A linear model was formulated to compare samples from aged and newborn mice, with chip number incorporated as a covariate. Adjusted p-values were computed employing FDR/BH correction to account for multiple comparisons. Annotation of differential methylation was based on the MouseMethylation-12v1-0_A2 manifest, and the assessment for p-value distribution was carried out via a QQ plot. Gene annotation of the MouseMethylation-12v1-0_A2 manifest was improved as described by Petkovich et al. (34). Briefly, CpG island locations were obtained from UCSC (https://hgdownload.soe.ucsc.edu). Shores and shelves were defined as regions 2 and 4 kb respectively upstream and downstream of the CpG islands. Ensembl annotated features (release 82, ftp.ensembl.org) were employed to identify promoters. Gene ontology (GO) analysis was performed on the significantly differentially methylated CpGs utilizing the R gprofiler2 package. Selection of GO terms related to aging was performed using https://geneontology.org/.

DNA methylation and transcriptome profiling (humans) – Data on chronic inactive demyelinated MS lesions and NAWM were sourced from our previous research, refer to Tiane et al., 2023 for detailed methodology (35). For details on demographics of the cohort refer to the supplementary information (Table S2)

Quantitative PCR – Total RNA, was isolated using the RNeasy Micro Kit (Qiagen, Venlo, The Netherlands) following lysis with Qiazol lysis reagent (Qiagen, The Netherlands). RNA concentration was assessed using a Nanodrop ND-2000 spectrophotometer (Isogen Life Science, De Meern, The Netherlands). Total RNA (>5 ng/µl) was reverse transcribed using the qScript cDNA SuperMix (Quanta Biosciences, Leuven, Belgium). qPCR was performed using the Applied Biosystems QuantStudio 3 Real-Time PCR System (Life Technologies, Gent, Belgium). Expression levels were normalized relative to two highly stable endogenous housekeeping genes (Table S3). The qPCR reaction was performed in a total volume of 10 µl, containing SYBR green master mix, 10 µM forward and reverse primers (Table S3), nuclease-free water, and 12.5 ng of template cDNA.

Immunohistochemistry (IHC) – Human post-mortem brain MS brain tissues were acquired from the Netherlands Brain Bank (http://www.brainbank.nl) (matrix number: MSMETH). Brain sections of 10 µm thickness, containing active/ remyelinated/ chronic inactive demyelinated lesions were prepared using a CM3050 S cryostat (Leica). Subsequently, samples were incubated with citrate buffer (0.1M in 0,1%PBS, pH 6.0) for antigen retrieval, starting at boiling temperature and allowing the buffer to cool to RT for 30 minutes. Next, sections were blocked in 10% donkey serum in PBS-T for 30 minutes at RT. Sections were incubated overnight at 4°C with OLIG2 and P16/ P21 primary antibodies (Table S1). The following day, slides were thoroughly washed and incubated with secondary Alexa 488 and 555-conjugated secondary antibodies for 1 hour at RT (Table S1). After nuclear staining with DAPI for 10 minutes, sections were mounted and visualized using a Leica DM2000 LED Microscope equipped with a Leica MC170 HD Camera (Leica Microsystems). Three random images were captured and averaged for lesions and NAWM of each tissue section. Image analysis was conducted using ImageJ-win64 software.

Glucose oxidase (GOx) treatment – Primary mouse OPCs were isolated from mixed glial cultures using the standard shake-off method. Isolated OPCs were maintained in culture and treated with different concentrations GOx (0, 30, 100, 300 mU) every 2 days over a 10-day period. For a detailed description, refer to the supporting information.

Statistical analysis – Statistical analysis and graph creation of experiments related to methylome and transcriptome profiling were performed using RStudio (version 2023.12.0), as described in the relevant sections. All other experiments were analyzed and graphed using GraphPad Prism 10.0.0 (GraphPad Software Inc., CA, USA). Normal distribution was verified with a Shapiro-Wilk test. Comparisons between two

group means were performed using a paired t-test for NAWM and lesions from the same patients; otherwise, an unpaired t-test was used. Continuous data are reported as means ± standard error of the mean (SEM). *p ≤ 0.05, **p < 0.01, ***p < 0.001, ****p < 0.0001.

RESULTS

Aging trends to reduce OPC proliferation capacity – Given the conflicting findings in previous research, we aimed to investigate how age affects the proliferation capacity of OPCs (36-38). To this end, we isolated nOPCs and aOPCs, and used PDGFRα and KI67 double immunolabeling to estimate the degree proliferation. Although not significant, there was a decreased trend (p = 0.0614) in the number of proliferating PDGFRα$^+$ cells in aged mice (Fig. 1A-C).

Dynamics of global DNA methylation patterns in aOPCs – Given that DNA methylation is a key element of aging, we analyzed differences in DNA methylation patterns between nOPCs and aOPCs (27, 39). PCA revealed that the separation of nOPCs and aOPCs was highly attributed to age (Fig. 2A). nOPCs clustered closely together while aOPCs formed a distinct, well-separated cluster. Staining for 5mC$^+$PDGFRα$^+$ cells showed no significant difference in the number of double positive cells (Fig 2B-D). However, by comparing average beta values aOPCs displayed global hypermethylation compared to nOPCs (Fig. 2E). Volcano plot analysis identified differential methylation in 35,796 out of 235,259 investigated CpG sites across the genome (LogFC <-1.5 or >1.5), representing nearly 15% of the sites (Fig. 2F-G). These differentially methylated CpG sites corresponded to 12,353 different genes, with approximately 74% of these CpGs located within a CpG island or its shores/shelves. Recognizing that the number of differentially methylated CpGs alone does not provide insight into their distribution, we performed a density analysis of the beta values. nOPCs showed a higher number of hypomethylated probes, while aOPCs were marked by hypermethylation (Fig. 2H).

DNA methylation sequencing reveals potential age-related epigenetic targets – Our gene set containing 12,353 differentially methylated genes was used for GO analysis, with a focus on 'Biological Processes' (Fig. 3A). Many differentially methylated patterns were attributable to developmental processes, including regulation of membrane potential, regulation of neurogenesis, and positive regulation of cell projection organization. As we are interested in aging, we narrowed down our focus to several GO terms that have been previously implicated in OPC aging (14, 18, 40, 41). Our 'aging analysis' included the following GO terms: cellular senescence (GO:0090398), oxidative stress (GO:0006979), telomeres (GO:0032204), and myelination (GO:0042552).

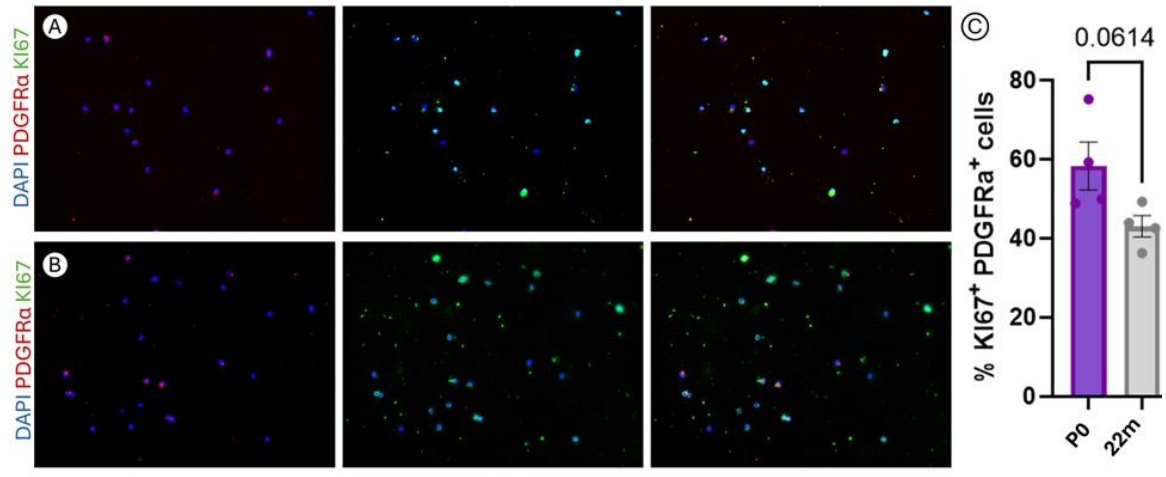

Fig. 1 – Decreasing trend in the proliferation capacity of aged OPCs. **A-C** Primary nOPCs and aOPCs were stained for PDGFRα, an early OPC marker, in combination with KI-67, a proliferation marker (n=4). OPCs, oligodendrocyte precursor cells; nOPCs, neonatal OPCs; aOPCs, aged OPCs ; PDGFRα, platelet-derived growth factor α; KI-67, antigen Kiel 67. Data are presented as mean ± SEM. 3 random images per sample. ns = non-significant, *p ≤ 0.05, **p < 0.01, ***p < 0.001, ****p < 0.0001; unpaired t-test.

Clustering based on the selected GO terms separated our samples based on age (Fig. 2B-E). We observed differential methylation in 302 different genes (Fig. 2F). Among these, for instance *Sirt2*, *P16*, *P21*, *Mbp*, and *Srf*, were previously described as hallmarks of aging in OPCs (14, 38, 42).

Sirtuin2 (SIRT2) as a target to epigenetically rejuvenate MS lesions – We aimed to investigate whether inflammation associated with MS is linked to accelerated epigenetic aging and how this impacts gene expression. While there were no global differences in DNA methylation patterns between lesions and NAWM (Fig. 4a), we observed an upregulation of DNMT3a when comparing MS brain samples to

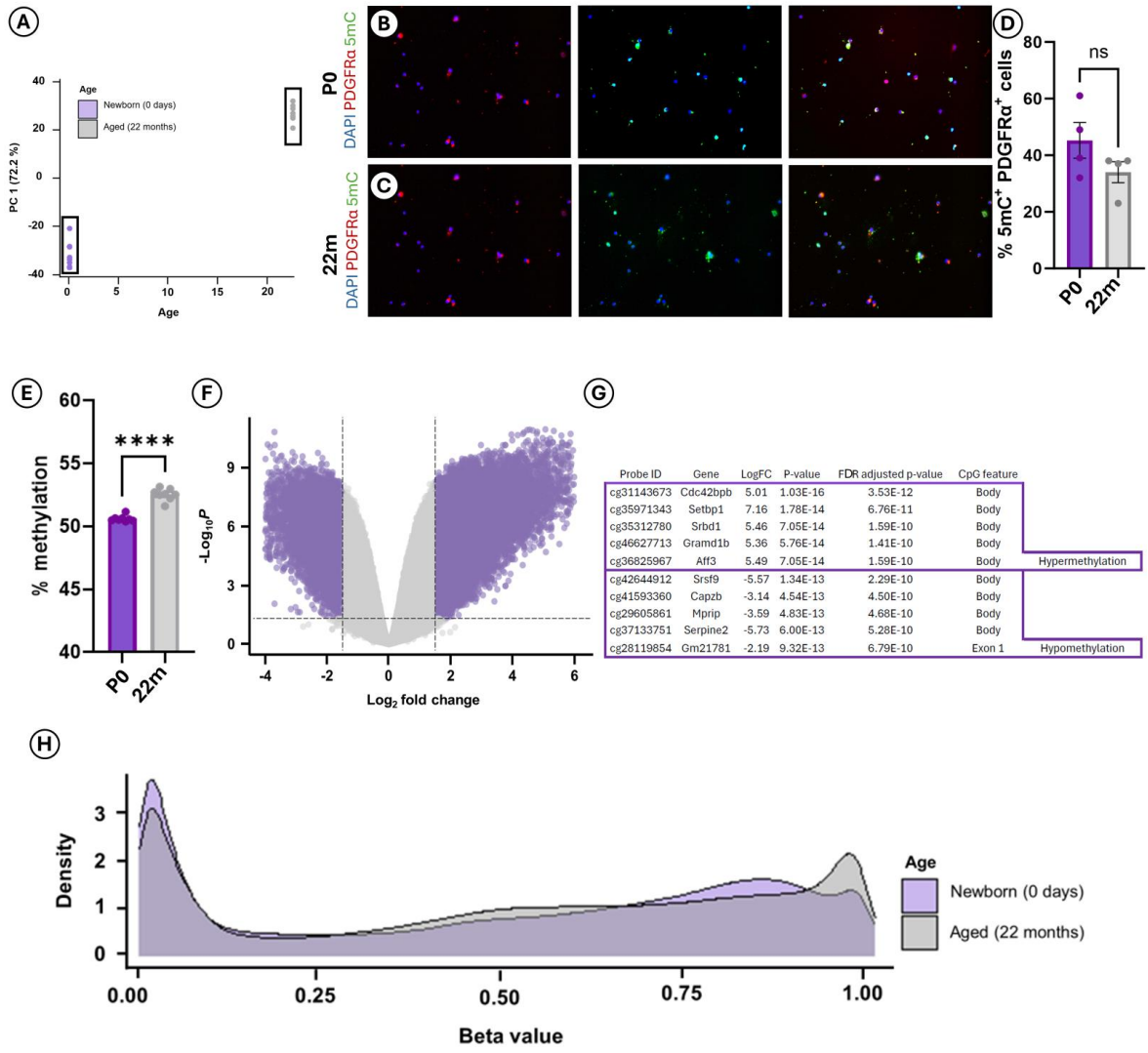

Fig. 2 – **OPCs show age-related shift in global DNA methylation patterns**. **A** Principal component analysis separates nOPCs and aOPCs based on age. **B-D** Primary mouse OPCs were stained for PDGFRα, an early OPC marker, in combination with 5mC, for global methylation (n = 4). **E** Differential methylation based on average beta values (n=8). **F** Volcano plot showing differentially methylated genes. Dashed lines represent P_{adj}=0.05 and LFC = (-)1.5 **G** The ten most significantly differentially methylated (hypermethylated and hypomethylated) CpGs located within CpG islands are listed. **H** Density plot showing age-associated differences in the distribution of DNA methylation patterns. OPC, oligodendrocyte precursor cell; nOPCs, neonatal OPCs; aOPCs, aged OPCs; PDGFRα, platelet-derived growth factor α; 5mC, 5-methylcytosine. LFC, $\log_2$ fold change. Data are presented as mean ± SEM. 3 random images per sample. ns = non-significant, *p ≤ 0.05, **p < 0.01, ***p < 0.001, ****p < 0.0001; unpaired t-test.

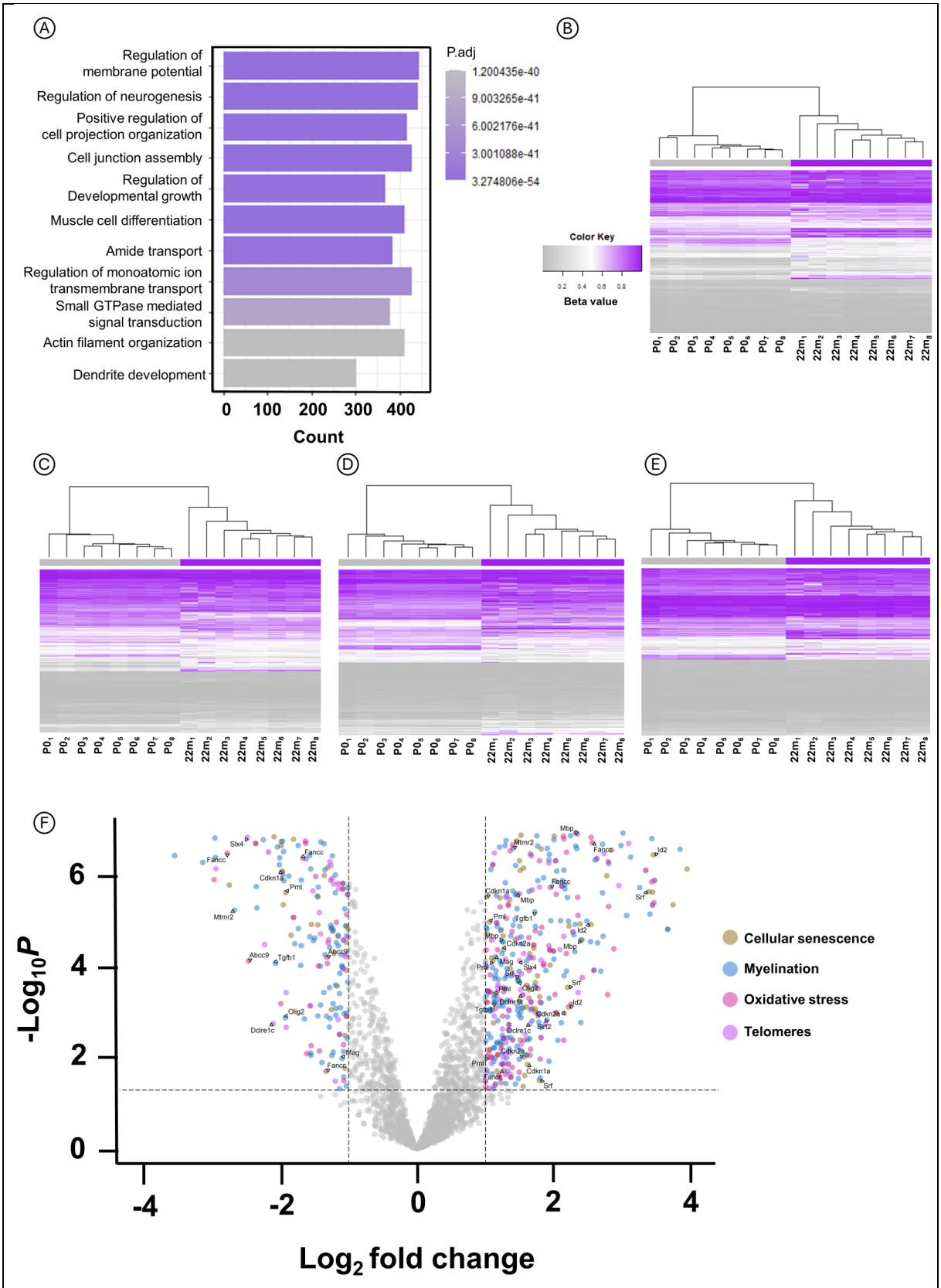

Fig. 3 – Age related changes in DNA methylation patterns of OPCs. **A** Gene ontology enrichment analysis shows the top 11 most significant gene ontologies. **B-E** Heatmaps for senescence (B), myelination (C), oxidative stress (D) and Telomeres (E) showing clustering of the samples based on age. **F** Volcano plot showing differentially methylated genes per gene ontology. Dashed lines represent Padj=0.05 and LFC = (-)1.5. P0, postnatal day 0; 22m, 22 months; OPCs, oligodendrocyte precursor cells; LFC, log_2 fold change.

non-neurologic control brain samples (Fig. S2A). Next, we performed GO analysis on the differentially methylated genes, revealing a significant enrichment of genes related to glial cells and myelination (Fig. 4B). To estimate epigenetic age acceleration, we compared the epigenetic age and chronological age of non-neurological controls to MS brain samples using the epigenetic clock developed by Shireby et al. The clock, specifically trained on cortical brain tissue, showed a trend towards increased epigenetic age acceleration (p=0.0966) in MS brain samples, indicating a greater difference between epigenetic and chronological age compared to control brain samples (Fig. 4C). Next, we examined the overlap between differentially methylated genes in mouse OPCs and MS samples to study the role of aging in MS disease progression. We only included genes that showed differential expression between lesions and NAWM. Interestingly, there was an overlap of 469 genes, 18 of which were associated with aging. Among these, methylation levels of the genes encoding for *MBP* and *SIRT2* showed a particularly strong negative correlation with their corresponding expression levels (Fig. 5A-B). Given our previous work on MBP methylation in MS progression (26), we focused on *SIRT2* in further analyses. *SIRT2*, also displayed differential methylation in aged mouse OPCs, and has previously been linked to OPC aging (38, 43). Seeking potential epigenetic targets to reverse epigenetic aging, we found a significant decrease in *SIRT2* expression in lesions compared to NAWM (Fig 5C), although qPCR validation between control and MS brain samples showed increased expression in MS samples (Fig. S2B). With a high correlation between methylation patterns and gene expression, we identified SIRT2 as a promising epigenetic target. Notably, *SIRT2* showed significant differential methylation between NAWM and lesions at nine CpG sites (Fig. 5D-E, S3). One CpG site in the TSS1500 region exhibited a very strong correlation with SIRT2 expression, highlighting its potential effect on gene expression (Fig 5F).

Increased number of senescent OPCs in lesions compared to NAWM – Previous research has identified P16 and P21 as key triggers of cellular senescence (14, 18, 24). Differential methylation analysis in mouse OPCs revealed hypermethylation in *P16* and *P21* genes in aOPCs However, between NAWM and lesions no significant differences in *P16*/ *P21* methylation and gene expression were found (data not shown). Since our differential methylation analysis is focused on bulk MS samples, we aimed to investigate P16 and P21 protein expression at the cellular level. Oligodendroglial lineage cells were identified using OLIG2 staining, and senescence was assessed with P16/P21 antibodies. Active lesions showed an increasing trend in the number of P21+ senescent OPCs compared to the surrounding NAWM (Fig. 6A-F). While there was no significant difference in the number of P16+ OPCs in active lesions, OPCs in remyelinated lesions displayed significantly higher P16 protein expression, and chronic inactive demyelinated lesions showed an increasing trend in P16 levels, supported by qPCR comparison with control samples (Fig. 6G-L, S2C). P21 levels did not significantly differ in chronic lesions compared to NAWM (Fig. 6M-O).

Oxidative stress-induced aging in OPCs – Interestingly it is known that cellular stress induced by reactive oxygen species (ROS) serves as a significant initiator of cellular senescence (44). Hence, nOPCs were subjected to GOx, an oxidizing enzyme that generates hydrogen peroxide through glucose oxidation (45). Following the culturing of nOPCs with four different GOx concentrations (0, 30, 100, 300 mU), increasing concentrations induced a dose-dependent increase in the expression of *P16* and *P21* (Fig. 7A-B). Moreover, considering that the aging process entails altered epigenetic mechanisms of gene regulation, we further examined the impact of GOx treatment on *Dnmt1* and *Dnmt3a* expression (Fig. 7C-D) (46). Again in a dose-dependent manner, GOx elevated the expression levels of the maintenance DNA methylation enzyme *Dnmt1* and the de novo methyltransferase *Dnmt3a*.

DISCUSSION

Aging has been pointed out as a major factor driving MS disease progression; however cellular and molecular mechanisms underlying the aging process are only poorly understood and therefore remain to be largely elucidated. Our epigenome-wide analysis revealed an age-related shift in DNA methylation patterns in aOPCs. Comparing differential methylation in aOPCs with MS brain samples, we found an association between aging and chronic MS lesions, manifested by alterations at both epigenetic and gene expression levels compared to NAWM.

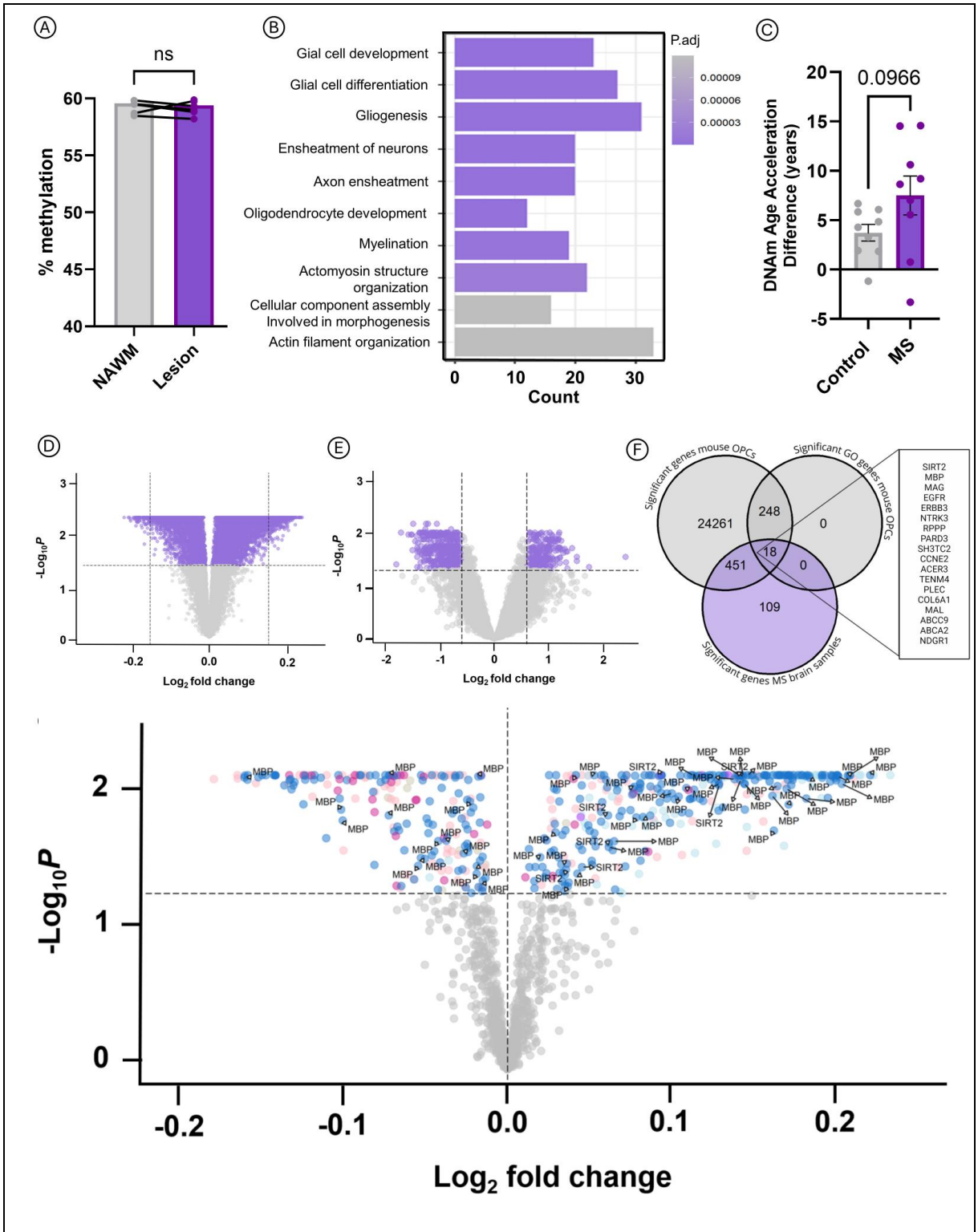

Fig. 4 – Differential methylation and expression of aging related genes in MS lesions. **A** No difference was indicated in global DNA methylation between NAWM and chronic inactive lesions (n=8). **B** Gene ontology enrichment analysis shows the top 10 most significant gene ontologies. **C** DNAm Age acceleration, based on the Cortical clock by shireby et al. DNAm age acceleration is calculated as the difference of chronological age and biological age (n=8-9). **D-E** Volcano plot showing differentially methylated (D) and expressed (E) genes. Dashed lines represent Padj=0.05 and LFC = (-) 0.1 (D) or (-) 0.5 (E). **F-G** Venn diagram (F) and volcano plot (G) showing genes that were differentially methylated in aOPCs and MS lesions. MS, multiple sclerosis; NAWM, normal-appearing white matter; LFC, $\log_2$ fold change. Data are presented as mean ± SEM. 3 random images per sample. ns = non-significant, *p ≤ 0.05, **p < 0.01, ***p < 0.001, ****p < 0.0001; paired t-test.

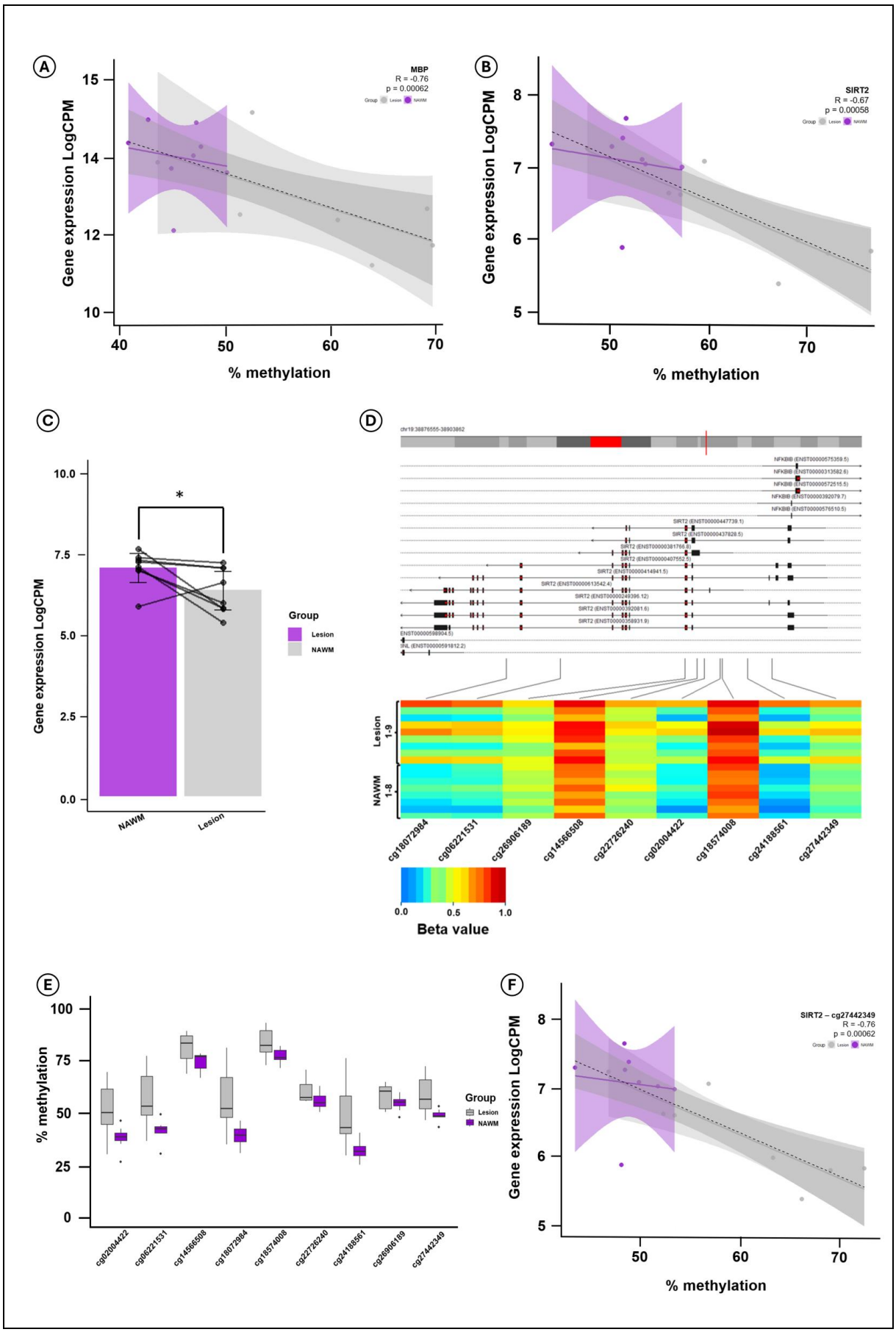
A
MBP
R = -0.76
p = 0.00062
Gene expression LogCPM
% methylation
B
SIRT2
R = -0.67
p = 0.00058
Gene expression LogCPM
% methylation
C
Gene expression LogCPM
Group
Lesion
NAWM
NAWM
Lesion
D
Lesion 1-9
NAWM 1-8
cg18072984
cg06221531
cg26906189
cg14566508
cg22726240
cg02004422
cg18574008
cg24188561
cg27442349
Beta value
E
% methylation
Group
Lesion
NAWM
F
SIRT2 – cg27442349
R = -0.76
p = 0.00062
Gene expression LogCPM
% methylation

Fig. 5 – Identifying SIRT2 as an epigenetic target in MS lesions. A-B Pearson's correlation shows a significant correlation between *SIRT* (A) and *MBP* (B) methylation and gene expression in NAWM and chronic inactive lesions. **C** Difference in *SIRT2* gene expression between NAWM and MS lesions. **D-E** VisualizeGene function (D) of the sesame package shows the distribution of differentially methylated CpGs of the *SIRT2* gene (E). **F** Potential epigenetic target in the TSS1500 of the *SIRT2* gene to epigenetically rejuvenate chronic inactive MS lesions. LogCPM, Log counts per million; SIRT2, Sirtuin 2; MS, multiple sclerosis; MBP, myelin basic protein; NAWM, normal-appearing white matter; TSS, transcription start site. Data are presented as mean ± SEM. *$p \leq 0.05$, **$p < 0.01$, ***$p < 0.001$, ****$p < 0.0001$; paired t-test.

We compared 12,353 differentially methylated genes between nOPCs and aOPCs with MS brains, and identified 469 of these genes showing differential methylation and expression between lesions and NAWM. A targeted approach focused on age-related GO terms revealed an overlap between 18 genes associated with senescence, myelination, oxidative stress, and telomeres. Remarkably, SIRT2 demonstrated hypermethylation in lesions, correlating with downregulated gene expression compared to NAWM, suggesting SIRT2 may serve as a promising target for epigenetic rejuvenation. In line with previous findings, both remyelinated and chronically demyelinated lesions exhibited heightened P16 levels compared to NAWM. Finally, we developed an in vitro model that partially mimics accelerated aging in mouse OPCs.

Given the ongoing discussion, we investigated whether the proliferation capacity of OPCs is affected by aging. Our findings indicate that aOPCs tend to lose proliferative capacity compared to nOPCs. This aligns with several murine studies showing a decline in OPC numbers during natural aging (36, 47, 48). Conversely a human post-mortem study reported a 12% decrease in OPC numbers during the initial 5 years of development, followed by stability throughout the entire lifespan, up to 90 years of age (37, 49). Research on monkey brains also revealed unchanged proliferative activity of OPCs with aging (38). The disparity in OPC numbers and proliferation capacity reported in different studies implies that the proliferative changes in aged OPCs may be contingent on the species and brain region assessed.

The CNS contains a substantial population of OPCs that generate OLs and repair myelin after demyelination. Studies on aged subjects show OPC differentiation capacity decreases with aging while demyelination increases (38). Aging leads to OPC dysfunction due to intrinsic and extrinsic factors such as DNA damage, reduced metabolic function, cellular senescence, and a differentiation-inhibiting environment, collectively contributing to OPC differentiation failure (40). Alterations in the epigenetic signature of cells, as a result of environmental changes are a major contributor to cellular aging. Starting from a zygote, a single cell gives rise to numerous different cell types, all containing the same DNA but exhibiting remarkable diversity due to the epigenetic regulation of gene expression. Next to alterations at the genomic and cellular level, the loss of epigenetic information is increasingly recognized as the primary driver of aging in mammals (50, 51). As first evidence by Horvath, and later on many others, DNA methylation is considered as a prediction model for biological age (52-54). Previous work has shown that DNA methylation is necessary for OPC differentiation and efficient remyelination after focal demyelination in murine (25, 28, 55, 56). During OPC differentiation *Dnmt3a* is upregulated, and its ablation was shown to impair OPC differentiation and remyelination (55). Zhou et al. demonstrated DNA methylation levels and the activity of DNMTs, particularly DNMT1 in OPCs derived from rat spinal cords decreased gradually with a age. Immunofluorescence revealed the number of $5mC^+PDGF\alpha^+$-positive OPCs between neonatal and aged mice did not differ. However, when comparing mean methylation values from our epigenomic analysis, we found increased myelination levels in aOPCs. Specifically, 12,353 genes were differentially methylated between nOPCs and aOPCs, nOPCs showing higher levels of hypomethylated probes, and aOPCs more hypermethylated probes. However, our results conflicted with previous findings that mouse-derived OPCs exhibit decreased 5mC methylation as they progress to adulthood (2 – 4 months) and age (22 months) (27, 28). The discrepancies may be due to the method of quantification; we only counted the number of high $5mC^+$ cells, whereas other studies measured

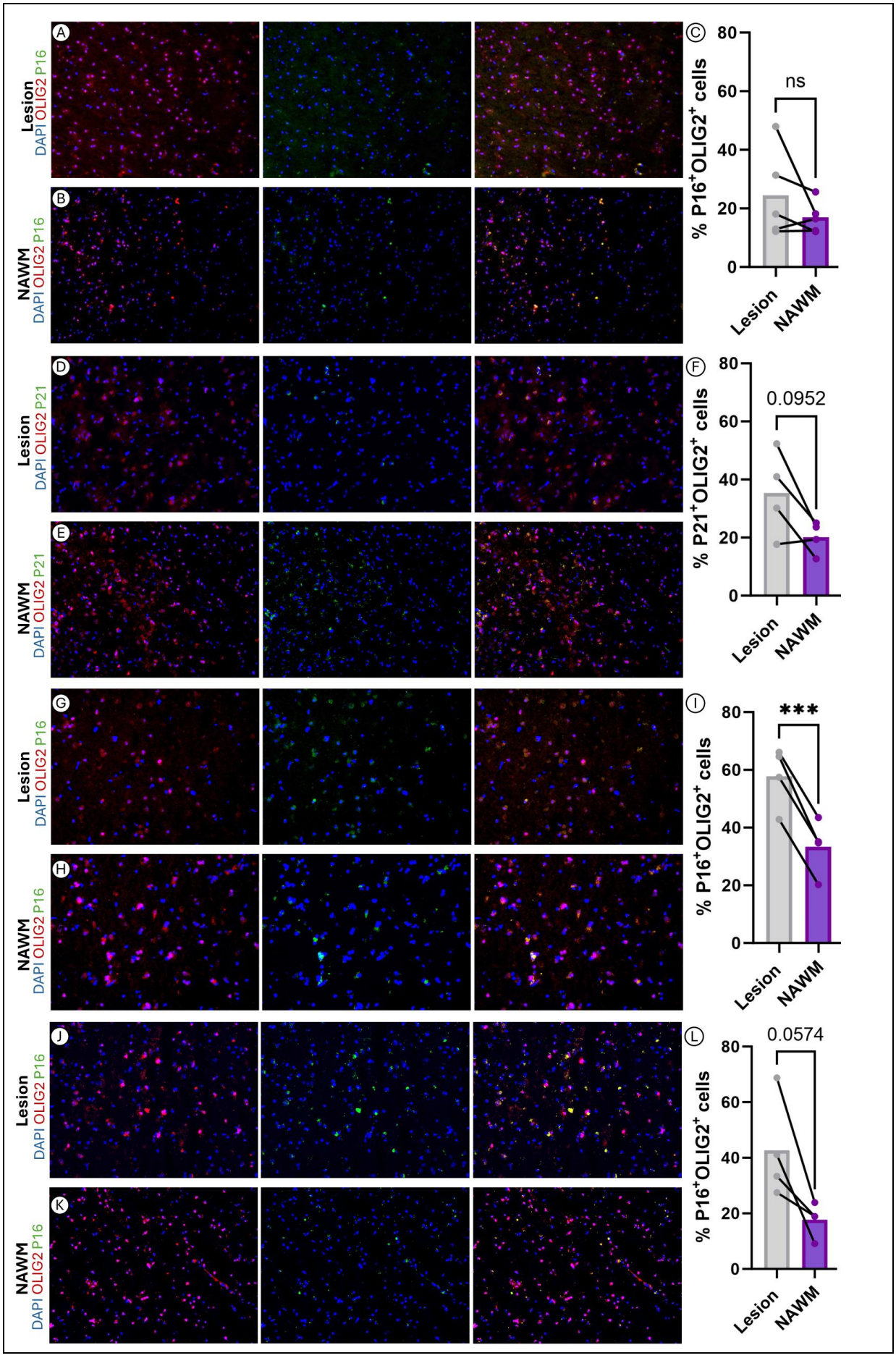
A
Lesion
DAPI OLIG2 P16
B
NAWM
DAPI OLIG2 P16
C
% P16+OLIG2+ cells
ns
Lesion
NAWM
D
Lesion
DAPI OLIG2 P21
E
NAWM
DAPI OLIG2 P21
F
% P21+OLIG2+ cells
0.0952
Lesion
NAWM
G
Lesion
DAPI OLIG2 P16
H
NAWM
DAPI OLIG2 P16
I
% P16+OLIG2+ cells
***
Lesion
NAWM
J
Lesion
DAPI OLIG2 P16
K
NAWM
DAPI OLIG2 P16
L
% P16+OLIG2+ cells
0.0574
Lesion
NAWM

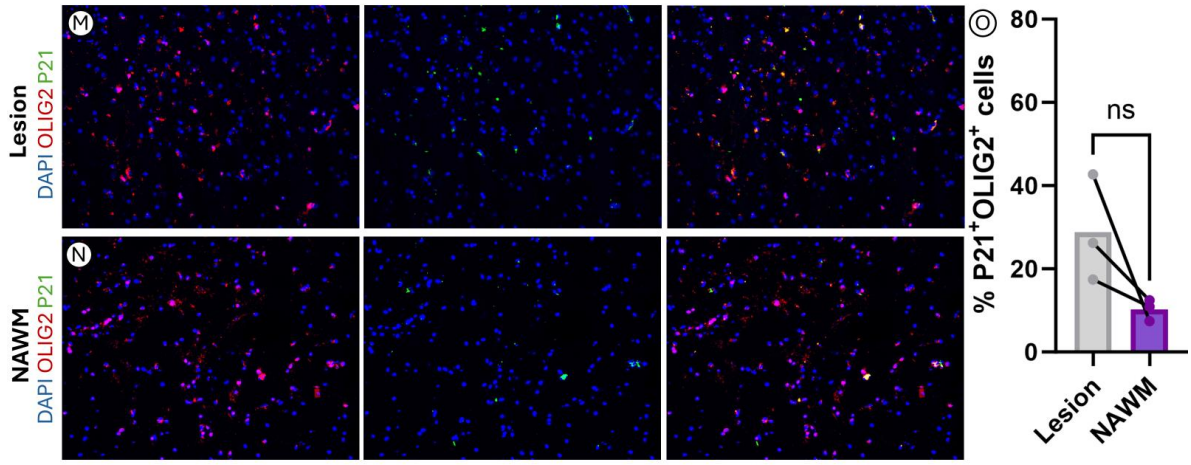

Fig. 6 - Lesion-derived OPCs are affected by senescence. Lesions and NAWM were stained for oligodendroglial marker OLIG2 and senescence markers P16/ P21. **A-F** Active lesions and NAWM were stained for senescence markers P16 (A-C) and P21 (D-F). **G-I** Remyelinated lesions and NAWM were stained for P16. **J-N** Chronic inactive demyelinated lesions and NAWM were stained for P16 (J-L) and P21 (M-O.) OLIG2, oligodendrocyte transcription factor 2; P16, protein 16: P21, protein 21; OPCs, oligodendrocyte precursor cells; NAWM, normal-appearing white matter. Data are presented as mean ± SEM (n=3-5). 3 random images per sample. *p ≤ 0.05, **p < 0.01, ***p < 0.001, ****p < 0.0001; paired t-test.

the staining intensity. Also, animals of different ages may account for the differences in results. Considering the high demand for myelination after birth, numerous changes to the methylome likely occur in early life (28, 57). The latter observation was also reflected in our GO enrichment analysis, showing high enrichment for genes related to development, such as the regulation of neurogenesis. Moreover, we confirmed that A2B5-specific MACS isolation achieves a high purity OPC isolate; however, the possibility of contamination with other cell types cannot be completely ruled out.

Focusing on aging we initiated our targetted analysis with genes previously associated with senescence, oxidative stress, telomeres, and myelination, which we showed clear clustering based on age. Among the 266 differentially methylated genes between nOPCs and aOPCs, senescence-associated genes *P16* and *P21*, both representing tumor suppressor and cell cycle regulators, have been designated to be important in the induction of cellular senescence in OPCs (24, 58). A study performed on the hippocampus of aged INK-ATTAC transgenic mice (aged 25-29 months), an inducible model to clear P16-positive senescent cells revealed that the OPC population exhibited the highest proportion of P16-positive cells. This was accompanied by elevated expression of the senescence marker P21 (24). Additionally, OPCs isolated from aged Sprague-Dawley rats (aged 20-24 months) demonstrated heightened *P16* expression (14). Genes related to myelination, such as *Srf*, *Mbp*, *Mag*, and *Olig2*, were also differentially methylated. Iram et al. found that *Srf* expression decreases in aged mouse-derived hippocampal OPCs (25 months), and that young cerebrospinal fluid (CSF) can restore normal levels and improve myelination, thereby enhancing long-term memory (42). Furthermore it was shown that *Mbp* expression was reduced in aged monkey brain-derived OLs (23 years) (38).

We did not directly link our findings regarding epigenetic alterations to gene expression levels in mice. Nevertheless, one of the strengths of this research is the cross-species analysis, as we compared our mouse data with human brain MS samples. In our MS brain analysis, we compared DNA methylation changes between lesions and NAWM of the same patients, which is a notable strength as it increased the power of our analysis. MS is known to be a highly heterogeneous disease, which complicates the analysis of its pathological features. By comparing lesions and NAWM from the same

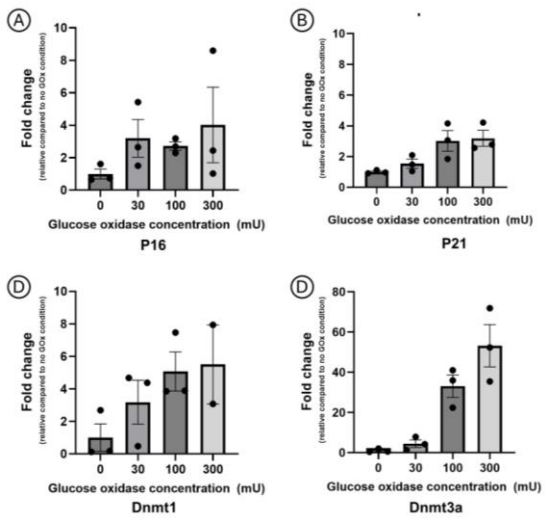

Fig. 7 - GOx as model to induce aging in OPCs. nOPCs were isolated and treated with different concentrations of GOx every 2 days, for a 10-day period **A-D** Gene expression of senescence markers *P21* (A) and *P16* (B) and DNA methylating enzymes *Dnmt1* (C) and *Dnmt3a* (D) after treatment of escalating concentrations GOx. Data are corrected for the most stable housekeeping genes (*Rpl13a* and *Cyca*). Data are presented as mean ± SEM. n=3/ group. GOx, glucose oxidase; OPC, oligodendrocyte precursor cell; nOPCs, neonatal OPCs; P21, protein 21; P16, protein 16; Dnmt, DNA methyl transferase.

patient we were able to investigate the differences between the lesions and their surrounding environment more accurately. Previous research has underscored the significant involvement of epigenetic aging in the progression of MS. Studies have demonstrated a marked increase in age acceleration within the glial cell population of MS patients compared to healthy controls (59). In our study, we aimed to compare the age-related changes in DNA methylation of aOPCs with those observed in MS. Although we did not observe differences in the global methylation values between lesions and NAWM, GO analysis revealed a notable enrichment in processes related to glial cells and remyelination. This finding aligns with the crucial roles played by microglia, astrocytes, and oligodendrocytes in the inflammatory response, myelin clearance, and myelin regeneration in MS (60, 61). An Epigenetic clock, predicting biological age based on DNA methylation at specific CpG sites, was employed to assess biological aging control- and MS brains. Our analysis hinted at accelerated epigenetic aging in lesions, suggesting a faster rate of biological aging within these regions. Nonetheless, this analysis has its limitations; it would have been preferable to differentiate between lesions and NAWM and even different types of lesions. Our investigations focused solely on chronic lesions to ensure clearer conclusions, however, exploring differences among various lesion types, which correspond to different disease stages, could have provided additional insights (59).

To further elucidate the role of aging in MS, we investigated similarities between differentially methylated genes in aOPCs and MS brain samples. We found an overlap in 469 genes, with 18 genes belonging to previously defined gene sets associated with aging processes. Notably, *MBP* and *SIRT2* exhibited a substantial number of differentially methylated probes, and demonstrated a strong negative correlation with their gene expression levels. Given our prior investigation into the role of MBP methylation (35), we focused on SIRT2, which displayed significantly lower expression in lesions compared to NAWM. Sirtuins comprise a family of Nicotinamide adenine dinucleotide (NAD+)-dependent deacetylases, consisting of seven members expressed in the brain, with Sirt2 being the most prevalent (62). Sirtuins are known for their role as a histone deacetylase, pivotal in maintaining genomic stability. Moreover, Sirt2 has been implicated in neurodegenerative diseases, with dysregulation contributing to the progression of Alzheimer's and Parkinson's diseases, often associated with aging (63, 64). While Sirt2 levels typically decline with age, studies on aged murine brains have yielded varied findings. Kireev et al. reported a decrease in *Sirt2* expression in the dentate gyrus of rats, whereas Braidy et al. found an increase in the occipital lobe, suggesting region-specific expression patterns (62, 65, 66). *Sirt2* exhibits particularly high proteolipid protein (PLP)-dependent expression in the oligodendrocyte lineage and is recognized for its crucial role in OPC differentiation and myelination (67). SIRT2 induces OPC differentiation by silencing *Pdgfrα* expression through the deacetylation of promoter-bound proteins, facilitating DNA methylation and gene silencing (68). The potential of SIRT2 in remyelination was confirmed in mouse OPCs, where restoring

nuclear entry of SIRT2 by supplementing an NAD+ precursor rescued OPC differentiation and remyelination in aged animals (43). We identified nine *SIRT2* CpGs that were hypermethylated in lesions compared to NAWM, with Cg27442349 located within the TSS1500, showing a high correlation with gene expression levels. Hence, we propose that targeting SIRT2 could hold promise as a way to epigenetically rejuvenate aging OPCs, thereby stimulating OPC differentiation and enhancing remyelination. A limitation of our study is that our investigation was restricted to MS bulk tissue, leaving unanswered questions regarding the applicability of these findings at the OPC level.

Previous research has highlighted elevated P16 levels in aged OPCs and precursor cells within MS lesions (4, 14). Our investigation uncovered distinct methylation patterns of P16 and P21 in aOPCs, while no disparities were detected in MS brain samples. Still, we sought to investigate differences at the protein level. In both remyelinated and chronic lesions, the number of P16+ OPCs was notably higher compared to the NAWM of the same patients. We observed a significant increase only in P16 levels within remyelinated lesions. This observation is likely attributable to the small sample size, which holds true for most of the stainings conducted in this study. The limited sample size may have compromised the statistical power of our analysis.

Finally, in order to investigate OPC aging *in vitro*, we established a model by subjecting neonatal OPCs to GOx treatment, a known inducer of oxidative stress. It is widely recognized that oxidative stress can trigger cellular senescence, as demonstrated in other glial cell types (69). We demonstrated that higher GOx concentrations resulted in increased expression of *P16* and *P21*. Contrarily higher GOx concentrations also elevated expression levels of DNA methylating enzymes DNMT1 and DNMT3a, which are typically reduced in aged cells (27). Therefore, while this model proves valuable for studying senescence in OPCs, it does not fully represent all aspects of the aging process, such as alterations in global methylation.

Building upon our findings regarding the aberrant methylation patterns of SIRT2 observed in MS lesions, our next research phase aims to investigate SIRT2 methylation and expression at the level of OPCs. We are currently optimizing NG2 staining as a preliminary step for laser capture microdissection-based (Fig. S1) OPC isolation from MS brain samples. Our primary goal is to employ CRISPR/dCas9 together with (de)methylating enzymes targeting SIRT2, to epigenetically rejuvenate aged OPCs within MS lesions. Additionally, we intend to investigate the downstream effects of SIRT2 deacetylating activity. With this knowledge we ultimately aim to stimulate OPC differentiation and promote remyelination, paving the way for novel therapeutic strategies to enhance remyelination in MS.

CONCLUSION

In summary, our study reveals significant changes in DNA methylation and gene expression associated with aging in MS lesions. We identified hypermethylation and downregulation of SIRT2 in MS lesions, suggesting its potential as a therapeutic target. Additionally, elevated levels of P16 in MS lesions compared to NAWM were observed. Our findings pave the way for future research aiming to rejuvenate aged OPCs and enhance remyelination in MS

REFERENCES

1. Walton C, King R, Rechtman L, Kaye W, Leray E, Marrie RA, et al. Rising prevalence of multiple sclerosis worldwide: Insights from the Atlas of MS, third edition. Mult Scler. 2020;26(14):1816-21.
2. Khan Z, Gupta GD, Mehan S. Cellular and Molecular Evidence of Multiple Sclerosis Diagnosis and Treatment Challenges. J Clin Med. 2023;12(13).
3. Koutsoudaki PN, Papadopoulos D, Passias PG, Koutsoudaki P, Gorgoulis VG. Cellular senescence and failure of myelin repair in multiple sclerosis. Mech Ageing Dev. 2020;192:111366.
4. Nicaise AM, Wagstaff LJ, Willis CM, Paisie C, Chandok H, Robson P, et al. Cellular senescence in progenitor cells contributes to diminished remyelination potential in progressive multiple sclerosis. Proc Natl Acad Sci U S A. 2019;116(18):9030-9.
5. Ghasemi N, Razavi S, Nikzad E. Multiple Sclerosis: Pathogenesis, Symptoms, Diagnoses and Cell-Based Therapy. Cell J. 2017;19(1):1-10.
6. Loma I, Heyman R. Multiple sclerosis: pathogenesis and treatment. Curr Neuropharmacol. 2011;9(3):409-16.
7. Neely SA, Williamson JM, Klingseisen A, Zoupi L, Early JJ, Williams A, et al. New oligodendrocytes exhibit more abundant and accurate myelin regeneration than those that survive demyelination. Nat Neurosci. 2022;25(4):415-20.
8. Yeung MSY, Djelloul M, Steiner E, Bernard S, Salehpour M, Possnert G, et al. Dynamics of oligodendrocyte generation in multiple sclerosis. Nature. 2019;566(7745):538-42.
9. Zhang X, Huang N, Xiao L, Wang F, Li T. Replenishing the Aged Brains: Targeting Oligodendrocytes and Myelination? Front Aging Neurosci. 2021;13:760200.
10. Cunniffe N, Coles A. Promoting remyelination in multiple sclerosis. J Neurol. 2021;268(1):30-44.
11. Klistorner A, Barnett M. Remyelination Trials: Are We Expecting the Unexpected? Neurol Neuroimmunol Neuroinflamm. 2021;8(6).
12. Sabsabi S, Mikhael E, Jalkh G, Macaron G, Rensel M. Clinical Evaluation of Siponimod for the Treatment of Secondary Progressive Multiple Sclerosis: Pathophysiology, Efficacy, Safety, Patient Acceptability and Adherence. Patient Prefer Adherence. 2022;16:1307-19.
13. de la Fuente AG, Queiroz RML, Ghosh T, McMurran CE, Cubillos JF, Bergles DE, et al. Changes in the Oligodendrocyte Progenitor Cell Proteome with Ageing. Mol Cell Proteomics. 2020;19(8):1281-302.
14. Neumann B, Baror R, Zhao C, Segel M, Dietmann S, Rawji KS, et al. Metformin Restores CNS Remyelination Capacity by Rejuvenating Aged Stem Cells. Cell Stem Cell. 2019;25(4):473-85 e8.
15. Munzel EJ, Becker CG, Becker T, Williams A. Zebrafish regenerate full thickness optic nerve myelin after demyelination, but this fails with increasing age. Acta Neuropathol Commun. 2014;2:77.
16. Gingele S, Henkel F, Heckers S, Moellenkamp TM, Hummert MW, Skripuletz T, et al. Delayed Demyelination and Impaired Remyelination in Aged Mice in the Cuprizone Model. Cells. 2020;9(4).
17. Sim FJ, Zhao C, Penderis J, Franklin RJ. The age-related decrease in CNS remyelination efficiency is attributable to an impairment of both oligodendrocyte progenitor recruitment and differentiation. J Neurosci. 2002;22(7):2451-9.

18. Windener F, Grewing L, Thomas C, Dorion MF, Otteken M, Kular L, et al. Physiological aging and inflammation-induced cellular senescence may contribute to oligodendroglial dysfunction in MS. Acta Neuropathol. 2024;147(1):82.
19. Zheng Q, Liu H, Yu W, Dong Y, Zhou L, Deng W, et al. Mechanical properties of the brain: Focus on the essential role of Piezo1-mediated mechanotransduction in the CNS. Brain Behav. 2023;13(9):e3136.
20. van Schaik PEM, Zuhorn IS, Baron W. Targeting Fibronectin to Overcome Remyelination Failure in Multiple Sclerosis: The Need for Brain- and Lesion-Targeted Drug Delivery. Int J Mol Sci. 2022;23(15).
21. Marschallinger J, Iram T, Zardeneta M, Lee SE, Lehallier B, Haney MS, et al. Lipid-droplet-accumulating microglia represent a dysfunctional and proinflammatory state in the aging brain. Nat Neurosci. 2020;23(2):194-208.
22. Tramontano A, Boffo FL, Russo G, De Rosa M, Iodice I, Pezone A. Methylation of the Suppressor Gene p16INK4a: Mechanism and Consequences. Biomolecules. 2020;10(3).
23. Fang JY, Lu YY. Effects of histone acetylation and DNA methylation on p21(WAF1) regulation. World J Gastroenterol. 2002;8(3):400-5.
24. Ogrodnik M, Evans SA, Fielder E, Victorelli S, Kruger P, Salmonowicz H, et al. Whole-body senescent cell clearance alleviates age-related brain inflammation and cognitive impairment in mice. Aging Cell. 2021;20(2):e13296.
25. Tiane A, Schepers M, Riemens R, Rombaut B, Vandormael P, Somers V, et al. DNA methylation regulates the expression of the negative transcriptional regulators ID2 and ID4 during OPC differentiation. Cell Mol Life Sci. 2021;78(19-20):6631-44.
26. Tiane A, Schepers M, Reijnders R, Veggel Lv. From methylation to myelination: epigenomic and transcriptomic profiling of chronic inactive demyelinated multiple sclerosis lesions. 2023.
27. Zhou J, Wu YC, Xiao BJ, Guo XD, Zheng QX, Wu B. Age-related Changes in the Global DNA Methylation Profile of Oligodendrocyte Progenitor Cells Derived from Rat Spinal Cords. Curr Med Sci. 2019;39(1):67-74.
28. Moyon S, Frawley R, Marechal D, Huang D, Marshall-Phelps KLH, Kegel L, et al. TET1-mediated DNA hydroxymethylation regulates adult remyelination in mice. Nat Commun. 2021;12(1):3359.
29. Moyon S, Ma D, Huynh JL, Coutts DJC, Zhao C, Casaccia P, et al. Efficient Remyelination Requires DNA Methylation. eNeuro. 2017;4(2).
30. Kular L, Ewing E, Needhamsen M, Pahlevan Kakhki M, Covacu R, Gomez-Cabrero D, et al. DNA methylation changes in glial cells of the normal-appearing white matter in Multiple Sclerosis patients. Epigenetics. 2022;17(11):1311-30.
31. Rouillard ME, Hu J, Sutter PA, Kim HW, Huang JK, Crocker SJ. The Cellular Senescence Factor Extracellular HMGB1 Directly Inhibits Oligodendrocyte Progenitor Cell Differentiation and Impairs CNS Remyelination. Front Cell Neurosci. 2022;16:833186.
32. Ding W, Kaur D, Horvath S, Zhou W. Comparative epigenome analysis using Infinium DNA methylation BeadChips. Brief Bioinform. 2023;24(1).
33. Ritchie ME, Phipson B, Wu D, Hu Y, Law CW, Shi W, et al. limma powers differential expression analyses for RNA-sequencing and microarray studies. Nucleic Acids Res. 2015;43(7):e47.
34. Petkovich DA, Podolskiy DI, Lobanov AV, Lee SG, Miller RA, Gladyshev VN. Using DNA Methylation Profiling to Evaluate Biological Age and Longevity Interventions. Cell Metab. 2017;25(4):954-60 e6.
35. Tiane A, Schepers M, Reijnders RA, Veggel Lv, Chenine S, Rombaut B, et al. From methylation to myelination: epigenomic and transcriptomic profiling of chronic inactive demyelinated multiple sclerosis lesions. bioRxiv. 2023:2023.01.12.523740.

36. Spitzer SO, Sitnikov S, Kamen Y, Evans KA, Kronenberg-Versteeg D, Dietmann S, et al. Oligodendrocyte Progenitor Cells Become Regionally Diverse and Heterogeneous with Age. Neuron. 2019;101(3):459-71 e5.
37. Yeung MS, Zdunek S, Bergmann O, Bernard S, Salehpour M, Alkass K, et al. Dynamics of oligodendrocyte generation and myelination in the human brain. Cell. 2014;159(4):766-74.
38. Dimovasili C, Fair AE, Garza IR, Batterman KV, Mortazavi F, Moore TL, et al. Aging compromises oligodendrocyte precursor cell maturation and efficient remyelination in the monkey brain. Geroscience. 2023;45(1):249-64.
39. Kaur G, Rathod SSS, Ghoneim MM, Alshehri S, Ahmad J, Mishra A, et al. DNA Methylation: A Promising Approach in Management of Alzheimer's Disease and Other Neurodegenerative Disorders. Biology (Basel). 2022;11(1).
40. Sams EC. Oligodendrocytes in the aging brain. Neuronal Signal. 2021;5(3):NS20210008.
41. Tiane A, Schepers M, Reijnders RA, van Veggel L, Chenine S, Rombaut B, et al. From methylation to myelination: epigenomic and transcriptomic profiling of chronic inactive demyelinated multiple sclerosis lesions. Acta Neuropathol. 2023;146(2):283-99.
42. Iram T, Kern F, Kaur A, Myneni S, Morningstar AR, Shin H, et al. Young CSF restores oligodendrogenesis and memory in aged mice via Fgf17. Nature. 2022;605(7910):509-15.
43. Ma XR, Zhu X, Xiao Y, Gu HM, Zheng SS, Li L, et al. Restoring nuclear entry of Sirtuin 2 in oligodendrocyte progenitor cells promotes remyelination during ageing. Nat Commun. 2022;13(1):1225.
44. Spaas J, van Veggel L, Schepers M, Tiane A, van Horssen J, Wilson DM, 3rd, et al. Oxidative stress and impaired oligodendrocyte precursor cell differentiation in neurological disorders. Cell Mol Life Sci. 2021;78(10):4615-37.
45. Khatami SH, Vakili O, Ahmadi N, Soltani Fard E, Mousavi P, Khalvati B, et al. Glucose oxidase: Applications, sources, and recombinant production. Biotechnol Appl Biochem. 2022;69(3):939-50.
46. Dansu DK, Sauma S, Huang D, Li M. The epigenetic landscape of oligodendrocyte progenitors changes with time. bioRxiv. 2024.
47. Segel M, Neumann B, Hill MFE, Weber IP, Viscomi C, Zhao C, et al. Niche stiffness underlies the ageing of central nervous system progenitor cells. Nature. 2019;573(7772):130-4.
48. Luan W, Qi X, Liang F, Zhang X, Jin Z, Shi L, et al. Microglia Impede Oligodendrocyte Generation in Aged Brain. J Inflamm Res. 2021;14:6813-31.
49. Wang F, Ren SY, Chen JF, Liu K, Li RX, Li ZF, et al. Myelin degeneration and diminished myelin renewal contribute to age-related deficits in memory. Nat Neurosci. 2020;23(4):481-6.
50. Wang K, Liu H, Hu Q, Wang L, Liu J, Zheng Z, et al. Epigenetic regulation of aging: implications for interventions of aging and diseases. Signal Transduct Target Ther. 2022;7(1):374.
51. Yang JH, Hayano M, Griffin PT, Amorim JA, Bonkowski MS, Apostolides JK, et al. Loss of epigenetic information as a cause of mammalian aging. Cell. 2024;187(5):1312-3.
52. Hannum G, Guinney J, Zhao L, Zhang L, Hughes G, Sadda S, et al. Genome-wide methylation profiles reveal quantitative views of human aging rates. Mol Cell. 2013;49(2):359-67.
53. Horvath S. DNA methylation age of human tissues and cell types. Genome Biol. 2013;14(10):R115.
54. Shireby GL, Davies JP, Francis PT, Burrage J, Walker EM, Neilson GWA, et al. Recalibrating the epigenetic clock: implications for assessing biological age in the human cortex. Brain. 2020;143(12):3763-75.

55. Moyon S, Casaccia P. DNA methylation in oligodendroglial cells during developmental myelination and in disease. Neurogenesis (Austin). 2017;4(1):e1270381.
56. Tiane A, Schepers M, Rombaut B, Hupperts R, Prickaerts J, Hellings N, et al. From OPC to Oligodendrocyte: An Epigenetic Journey. Cells. 2019;8(10).
57. Sturrock RR. Myelination of the mouse corpus callosum. Neuropathol Appl Neurobiol. 1980;6(6):415-20.
58. Safwan-Zaiter H, Wagner N, Wagner KD. P16INK4A-More Than a Senescence Marker. Life (Basel). 2022;12(9).
59. Kular L, Klose D, Urdanoz-Casado A, Ewing E, Planell N, Gomez-Cabrero D, et al. Epigenetic clock indicates accelerated aging in glial cells of progressive multiple sclerosis patients. Front Aging Neurosci. 2022;14:926468.
60. Luo C, Jian C, Liao Y, Huang Q, Wu Y, Liu X, et al. The role of microglia in multiple sclerosis. Neuropsychiatr Dis Treat. 2017;13:1661-7.
61. Ponath G, Park C, Pitt D. The Role of Astrocytes in Multiple Sclerosis. Front Immunol. 2018;9:217.
62. Sidorova-Darmos E, Wither RG, Shulyakova N, Fisher C, Ratnam M, Aarts M, et al. Differential expression of sirtuin family members in the developing, adult, and aged rat brain. Front Aging Neurosci. 2014;6:333.
63. Liu Y, Zhang Y, Zhu K, Chi S, Wang C, Xie A. Emerging Role of Sirtuin 2 in Parkinson's Disease. Front Aging Neurosci. 2019;11:372.
64. Sola-Sevilla N, Puerta E. SIRT2 as a potential new therapeutic target for Alzheimer's disease. Neural Regen Res. 2024;19(1):124-31.
65. Kireev RA, Vara E, Tresguerres JA. Growth hormone and melatonin prevent age-related alteration in apoptosis processes in the dentate gyrus of male rats. Biogerontology. 2013;14(4):431-42.
66. Braidy N, Poljak A, Grant R, Jayasena T, Mansour H, Chan-Ling T, et al. Differential expression of sirtuins in the aging rat brain. Front Cell Neurosci. 2015;9:167.
67. Werner HB, Kuhlmann K, Shen S, Uecker M, Schardt A, Dimova K, et al. Proteolipid protein is required for transport of sirtuin 2 into CNS myelin. J Neurosci. 2007;27(29):7717-30.
68. Fang N, Cheng J, Zhang C, Chen K, Zhang C, Hu Z, et al. Sirt2 epigenetically down-regulates PDGFRalpha expression and promotes CG4 cell differentiation. Cell Cycle. 2019;18(10):1095-109.
69. Bitto A, Sell C, Crowe E, Lorenzini A, Malaguti M, Hrelia S, et al. Stress-induced senescence in human and rodent astrocytes. Exp Cell Res. 2010;316(17):2961-8.

Acknowledgements – I would like to express my deepest gratitude to Assia Tiane, my daily supervisor, for her invaluable assistance with my experiments and writing and allowing me to pursue my own research ideas. I extend my sincere thanks to Daniel van den Hove and Tim Vanmierlo, my promoters from Maastricht and Hasselt University, for giving me the opportunity to conduct my research within their team and for their support during my internship and thesis writing. I am also very grateful to Lisa Koole, who took over as my daily supervisor, assisted me during my experiments in the lab, and greatly enhanced my R programming skills. Furthermore, I would like to thank Inez Wens and Melissa Schepers for their support in thesis writing and the constructive feedback they provided. Finally, I want to express my gratitude to my friends and family, with special appreciation for my significant other.

Author contributions – T.V. and A.T. were responsible for the design of my internship project. F.L., L.K. and A.T. executed the lab experiments and data analysis. Manuscript writing was performed by F.L. under supervision of A.T. and I.

SUPPLEMENTAL INFORMATION

METHODS

Shake-off - Mouse cortices were mechanical and enzymatic digested using surgical equipment and papain solution (30 minutes, 37°C) (3U/ml, diluted in Dulbecco's Modified Eagle Medium (DMEM) supplemented with 1 mM L-cysteine; Sigma-Aldrich, Bornem, Belgium). Mixed glial cells were maintained in DMEM (SigmaAldrich), supplemented with 50U/ml penicillin and 50 mg/ml streptomycin (P/S; Invitrogen, Merelbeke, Belgium) and 10% heat-inactivated fetal calf serum (FCS; Hyclone, Erebodegem, Belgium) on poly-l-lysine-coated (5 µg/ml, Sigma-Aldrich) culture flasks (37°C, 8,5% CO_2). From the seventh day, culture medium was supplemented with insulin (5 µg/ml; Sigma-Aldrich) to stimulate OPC formation. On day 14, the cells were shaken using an orbital shaker (75 rpm, 37 °C, 45 min) to detach the microglial layer. After a second shake-off (16 hours, 250 rpm), the supernatant containing the OPCs was incubated for 20 minutes on a petri-dish and centrifuged (300xg, 5 minutes. Isolated OPCs were then further maintained in culture, and treated with varying GO concentrations (0, 30, 100, 300 mU) every 2 days. On day 10, OPCs were used for RNA isolation and cDNA synthesis as described in the relevant sections.

Laser capture microdissection (LCM) test stainings – Ten-micrometer acetone-fixed cryosections were fixed in ice-cold acetone for 10 minutes and then dip-washed in TBS, TBS-T, and TBS. After blocking for 20 minutes with 10% donkey serum in 0.1% PBS, the slices were incubated with primary antibodies against NG2 and p16 (Table S1) for 20 minutes at RT. The primary antibodies were detected using donkey anti-goat Alexa 566 and donkey anti-rabbit Alexa 488 secondary antibodies (Table S1) for 6 minutes at RT, with DAPI used for nuclear staining. For details on the long staining protocol, refer to the IHC section.

RESULTS

LCM test staining identified NG2 as the most promising marker for OPC isolation – While our current study focused on analyzing methylation differences in bulk brain tissue, our future direction involves OPC-level analyses. To support this, we stained control and chronically demyelinated brain tissue using two well-known OPC markers, NG2 and PE-conjugated A2B5 (Table S…). Initially, we stained healthy control brain tissue for NG2 and A2B5, comparing a shortened staining protocol to the standard procedure. NG2 emerged as the most promising marker, exhibiting minimal background staining. Subsequently, we tested different concentrations of donkey serum as a blocking agent for NG2 staining in chronically demyelinated MS lesions. Optimal staining was achieved with 10% donkey serum. Therefore, we will continue with NG2 staining using 10% donkey serum. Further optimization is still required, as the signal intensity was insufficient for isolating NG2+ cells using LCM.

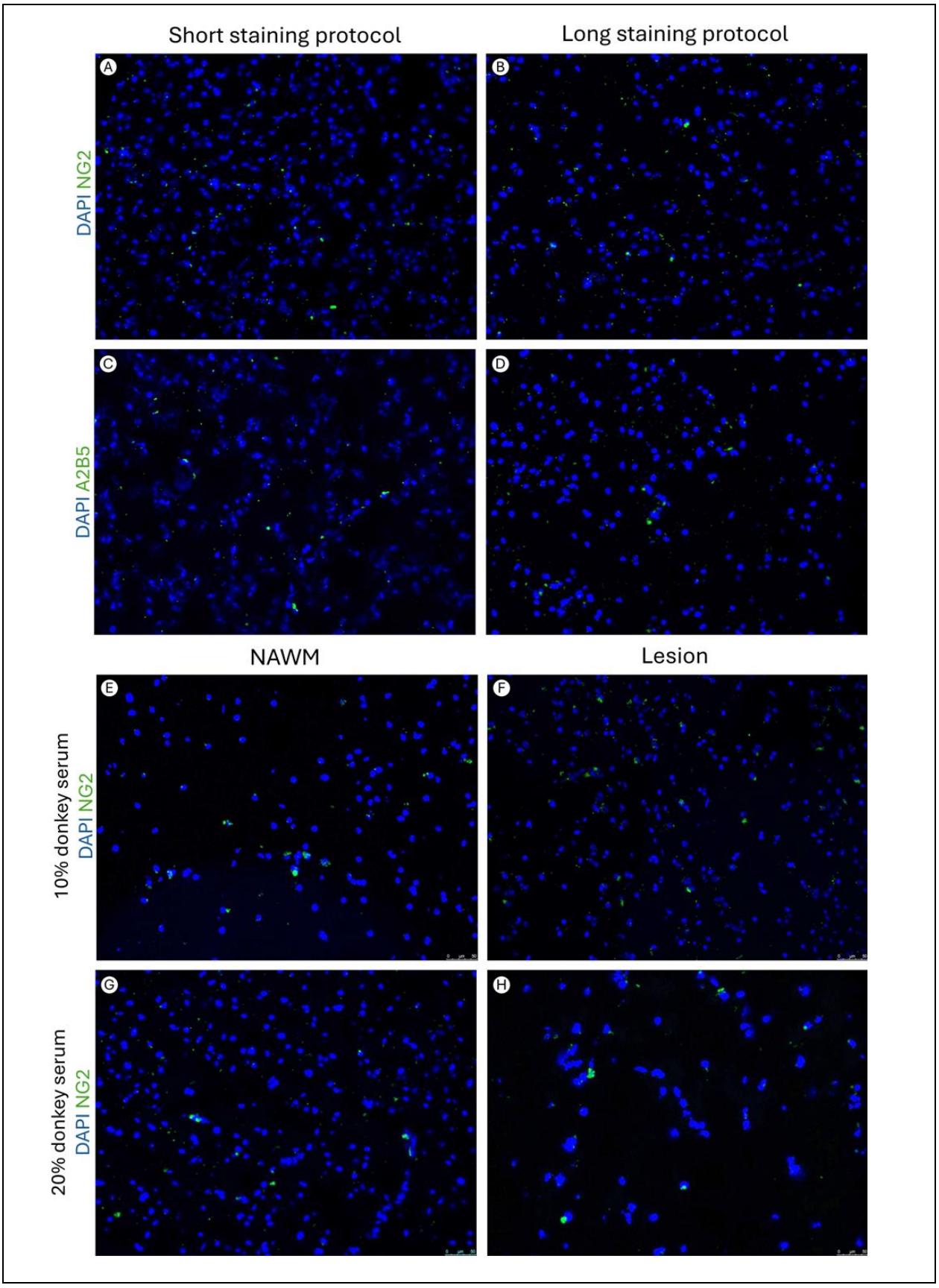
Short staining protocol
Long staining protocol
A
B
DAPI NG2
C
D
DAPI A2B5
NAWM
Lesion
E
F
10% donkey serum
DAPI NG2
G
H
20% donkey serum
DAPI NG2

Fig. S1 - LCM test staining. Healthy brain control tissue were stained for NG2 (A-B) or A2B5 (C-D) to determine the optimal marker for OPC labeling. Since LCM requires a short staining protocol to preserve the integrity of genomic material, we compared a short staining protocol (A,C) with a standard long protocol (B,D). **E-H** Comparison of 10% (E-F) vs. 20% (G-H) donkey serum blocking agent in NAWM (E,G) vs. Chronic inactive demyelinated MS lesions (F,H). NG2, neural/glial antigen 2; A2B5, A2B5 antigen; LCM, laser capture microdissection; MS, multiple sclerosis; OPC, oligodendrocyte precursor cell; NAWM, normal-appearing white matter.

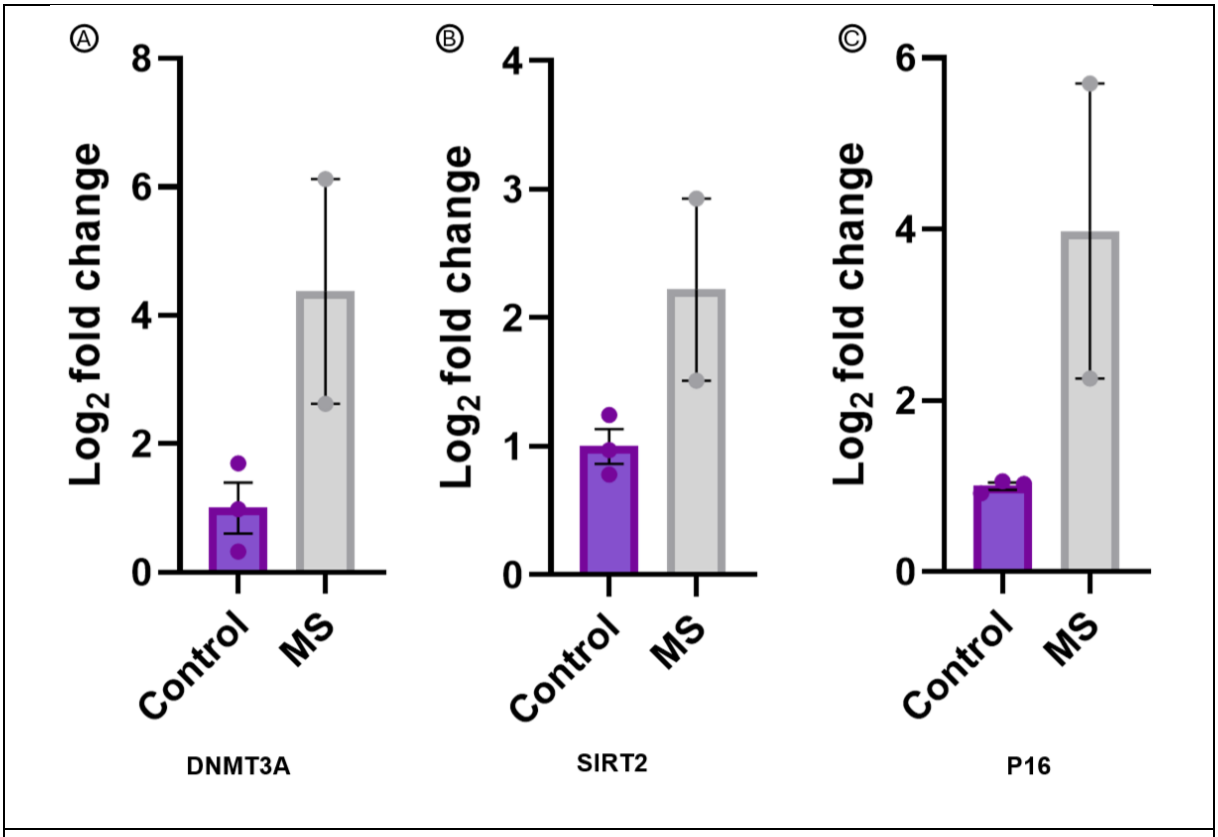

Fig. S2 – qPCR analysis of differential gene expression between control brain samples and bulk MS tissue containing chronic inactive demyelinated lesions. A-C Difference in gene expression of *DNMT3A* (A), *SIRT2* (B) and *P16* (C) between control and MS samples. MS, Multiple sclerosis; DNMT3A, DNA methyl transferase 3a; P16, protein 16.

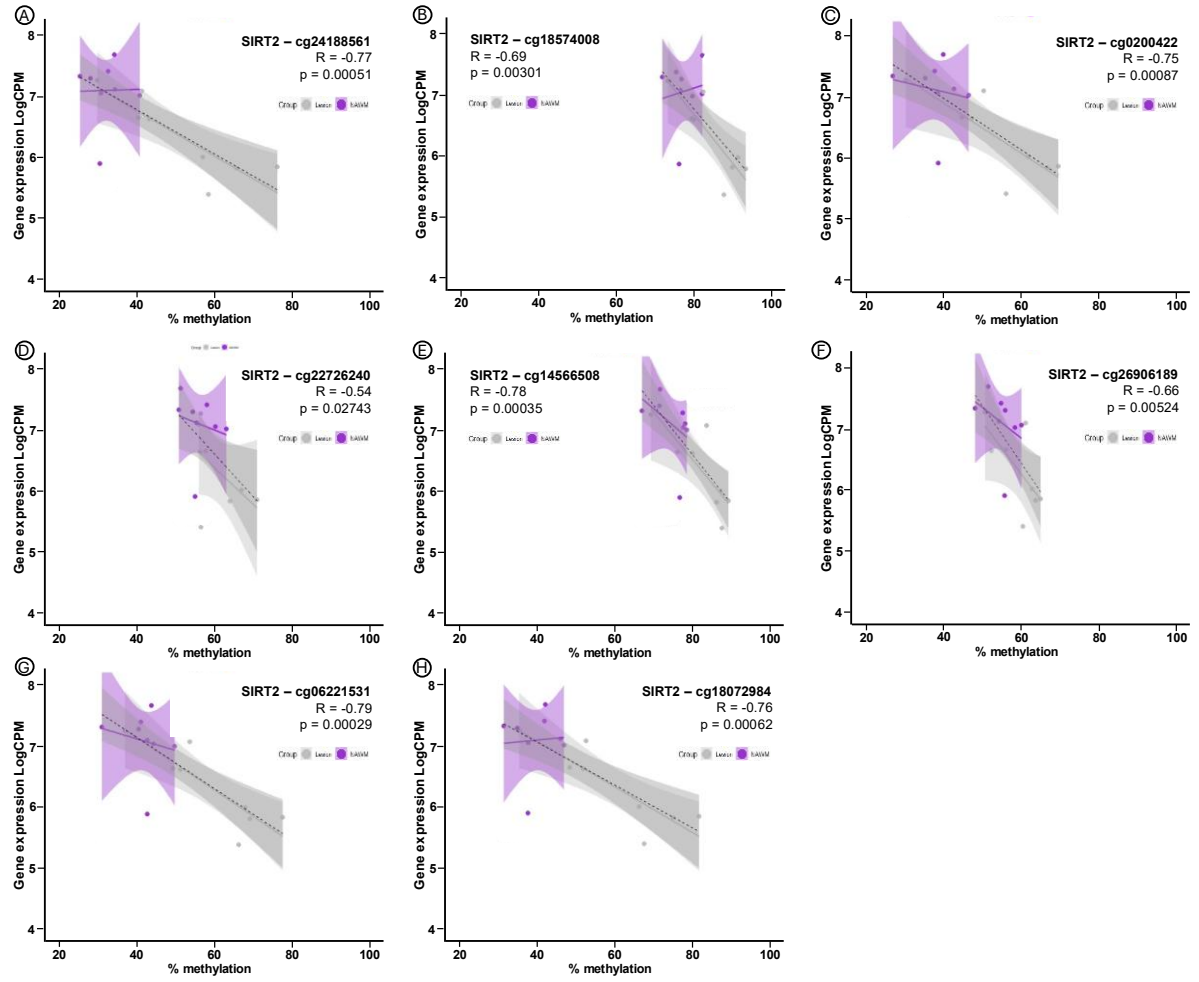

Fig. S3 - Identifying SIRT2 as an epigenetic target in MS lesions. A-H Pearson's correlation shows the significant correlation between *SIRT2* methylation and gene expression at several CpGs in NAWM and chronic inactive lesions. LogCPM, log count per million; SIRT2, Sirtuin2; MS, multiple sclerosis; NAWM, normal-appearing white matter.

Table S1 – List of antibodies used for immunofluorescence

Primary antibodies		
Reagent	**Source**	**Identifier**
Goat anti-olig2	RnD systems, MN, USA	Cat #AF2418
Rabbit anti- p16	Proteintech, IL, USA	Cat #10883-AP
Rabbit anti-p21	Proteintech	Cat #28248-1-AP
Rabbit anti-Ki67	Abcam, Cambridge, UK	Cat #ab15580
Mouse anti-5mC	Abcam	Cat #ab10805
Rabbit anti-NG2	Abcam	Cat #ab83178
PE-conjugated A2B5	Miltenyi Biotec, Leiden, The Netherlands	Cat #130-123-715
Secondary antibodies		
Reagent	**Source**	**Identifier**
Goat anti-rabbit, Alexa 488	Invitrogen, MS, USA	Cat #A21206
Donkey anti-goat, Alexa 555	Invitrogen	Cat #A21432
Nuclear staining		
Reagent	**Source**	**Identifier**

4,6′ -diamidino-2-phenylindole	Sigma-Aldrich, Hoeilaart, Belgium	Cat #D9542

Table S2 – demographics of the human cohort

Characteristics	Non-neurological controls	MS patients
Gender (male/ female)	4/6	4/6
Age, mean (SD)	65.7 (8.90)	64.7 (9.64)
Disease diagnosis (PPMS/ PRMS/ SPMS/ unspecified)	N.a.	3/1/4/2
PMI, mean (SD)	9.12 (1.87)	9.72 (4.09)

SD, standard deviation; PPMS, primary progressive multiple sclerosis (MS); PRMS, progressive relapsing MS; SPMS, secondary progressive MS; PMI, postmortem interval.

Table S3 – list of primers used for qPCR

Human primers **Gene**	**Forward primer**	**Reverse primer**
SIRT2	ACGGCACCTTCTACACATCACA	AGATCTTCTCTTTCATCCAGCTTAGC
DNMT1	CCCCTGAGCCCTACCGAAT	CTCGCTGGAGTGGACTTGTG
DNMT3a	TATTGATGAGCGCACAAGAGAGC	GGGTGTTCCAGGGTAACATTGAG
P16	GAAGGTCCCTCAGACATCCCC	CCCTGTAGGACCTTCGGTGAC
RPL13A (HK)	AAGTTGAAGTACCTGGCTTTCC	GCCGTCAAACACCTTGAGAC
YWAZ (HK)	CTTGACATTGTGGACATCGG	TATTTGTGGGACAGCATGGA
Mouse primers **Gene**	**Forward primer**	**Reverse primer**
Dnmt1	GACAGTGACACCCTTTCAGTTG	GAAGTGAGCCGTGATGGTG
Dnmt3a	CTGGCTCTTTGAGAATGTGG	TGCAGCAGACACTTCTTTGG
P16	GTGATGTCCGACCTGTTCCG	CCACGGGACCGAAGAGACAA
P21	TCGTACCCCGATTCAGGTGAT	TAGTGGGGTCCTCGCAGTT
Rpl13a (HK)	GGATCCCTCCACCCTATGACA	CTGGTACTTCCACCCGACCTC
Cyca (HK)	ACGTCTCCTTCGAGCTGTT	AAGTCACCACCCTGGCA

HK, housekeeping.